X-ray analysis of protective coatings

Zoestbergen, Edzo

4 Profound diffraction study of TiN

The diffraction experiments of the previous section have revealed some general properties of the coatings. However, the picture is far from complete. To determine the residual stresses the measurements of the lattice spacing in section 3.2 were carried out on the {220} reflections. The main reason for choosing this particular plane was the linear relation that exists between the lattice spacing and the $\sin^2\psi$. However, the relation between the {200} planes and the $\sin^2\psi$ is not linear.

The specimens from the second batch show a d-$\sin^2\psi$ behaviour that is oscillatory. This behaviour seems related to the texture and is studied extensively in the first section of this chapter.

A non-linear d-$\sin^2\psi$ relation is also found in the {200} planes of the specimens from the third batch. These specimens have a curved d-$\sin^2\psi$ relation, which is also present in the commercially produced TiN coatings, i.e. all the specimens with a high deformation strain. This non-linearity is not related to the texture. To investigate this behaviour and also the high deformation strain that is present in these specimens a commercial TiN film is isolated from the substrate and the change in residual stress and deformation strain are investigated, section 4.2. Besides this, annealing experiments are carried out on the specimens of the third batch to study the change in relation between the lattice spacing and the $\sin^2\psi$ and to try to clarify the high deformation strain that are present in these specimens, section 4.3.

4.1 The influence of atomic peening during magnetron sputtering on the crystallographic texture and the d-$\sin^2\psi$ relation.

Introduction

In this section the magnetron sputtered TiN layers of the second batch are thoroughly investigated. The crystallographic texture in these specimens is biaxial and the strain measurements, carried out on the {200} planes, exhibit a non-linear d-$\sin^2\psi$ behaviour, which is not present for the {220} planes, Figure 4.1. The oscillatory behaviour in the {200} planes cannot be explained by the well-known causes of an oscillatory d-$\sin^2\psi$ relation, i.e. like anisotropic X-ray elastic constants in combination with a strong texture or the presence of shear stresses. (See the discussion at the end of section 4.1.1) Assuming that the

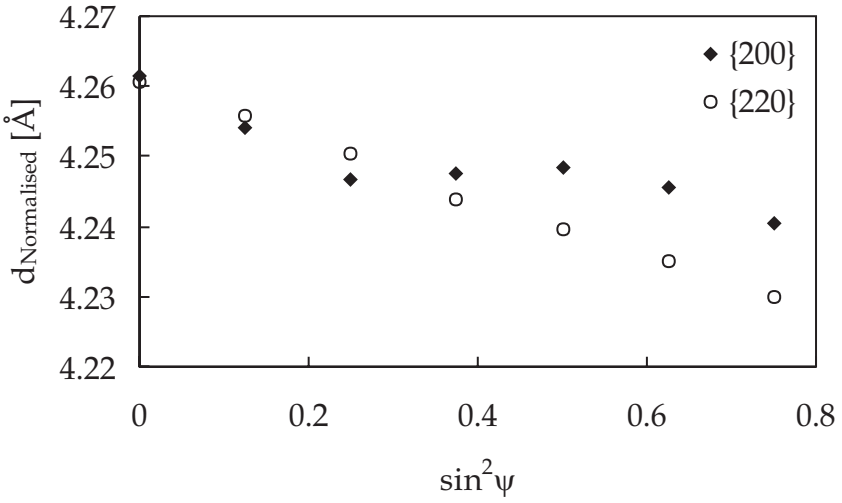

Figure 4.1 Normalised lattice spacings of the {200} and the {220} planes. Film thickness is 2 µm. Only the {220} planes show a linear d-$\sin^2\psi$ relation.

driving force behind the texture evolution is the ion-bombardment during sputtering (section 3.3.1), then the texture is a consequence of the dependence of the sputtering yield on grain orientation. This process may also have an influence on the atomic peening process, which is the main cause of stress generation. Grains with a higher peening ratio, i.e. the right orientation, will have a lattice spacing that is larger than other grains. This is due to the effect of the peening, which generates a hydrostatic stress in the grains. The non-linear

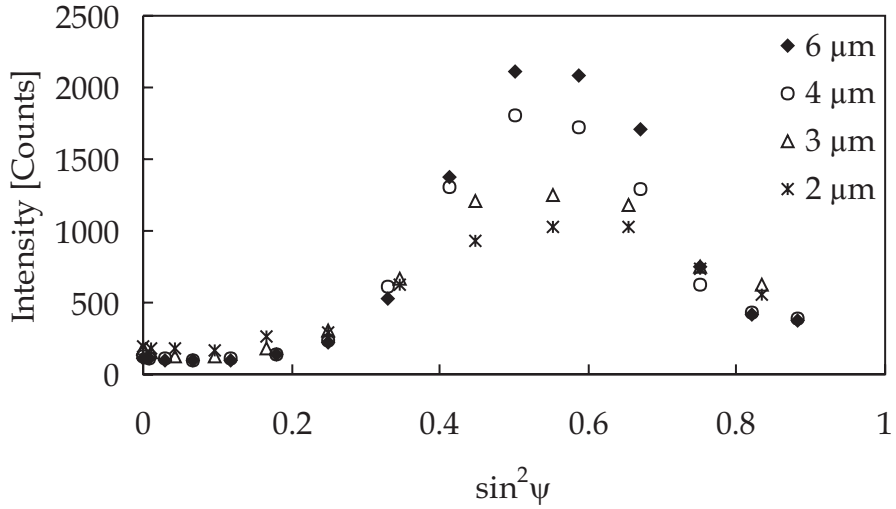

Figure 4.2 The intensities of the {200} reflections of the four specimens measured in the rolling direction show that there is a texture gradient present.

$\sin^2\psi$ relation can now be explained, taking the texture and this atomic peening properly into account.

4.1.1 Measurements

Texture

The specimens from the second batch all have a biaxial texture and the only difference between the specimens is the intensity distribution. In Figure 4.2 the peak intensity of the {200} reflections in the rolling direction are plotted versus the $\sin^2\psi$. Table 4.1 contains the maximum measured intensity and the intensity at ψ=0 for the four specimens. The measured intensities are corrected for background effects, defocus effects and the difference in coating thickness. The maximum intensity increases and the intensity at ψ=0 decreases with increasing layer thickness. Assuming no changes in the grain size, defect density and that the picture at lower thickness is preserved when a longer deposition time is used, it can be concluded that a texture development is taking place in the layer and there exists a texture gradient in the coating. The biaxial texture was explained in chapter 3, by assuming that the ion-bombardment and kinetic effects play the key-role in the development of the texture. For the ion-bombardment the selection mechanism for grain orientation is the difference in sputtering yield between grains. Therefore, the resputtering is lower for aligned grains than for misaligned grains.

Table 4.1 The intensity at ψ=0° and the maximum intensity

	Intensity	
Film thickness [μm]	Maximum	ψ=0
2	1050	178
3	1300	147
4	1850	110
6	2300	98

Strain measurements

The *d*-spacings of the {200} planes are measured as a function of $\sin^2\psi$. This is done in two different φ directions: in the rolling and the transverse direction. In Figure 4.3 the results from the measurements on the 30 minutes specimen are plotted. There is a clear difference between the two directions: for the transverse direction there is more or less a linear relation, between the *d*-spacing and the

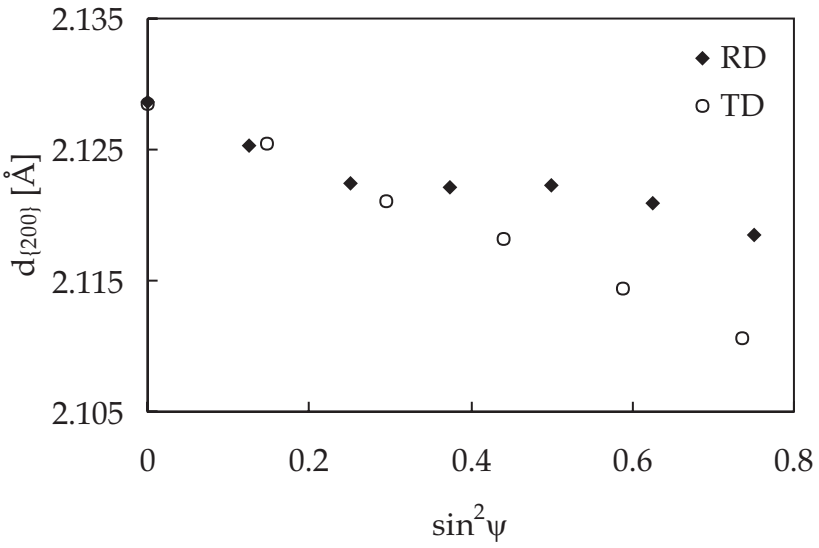

Figure 4.3 Lattice spacing of the {200} planes. Film thickness is 2 µm. The oscillation is visible in the rolling direction and the d-$\sin^2\psi$ relation is almost linear in the transverse direction.

$\sin^2\psi$, which is in contrast with the results for the rolling direction, where the d-$\sin^2\psi$ graph shows an oscillatory behaviour.

In Figure 4.4 the d-spacings for the four specimens, measured in the rolling direction, are plotted versus the $\sin^2\psi$. They all show this non-linear behaviour

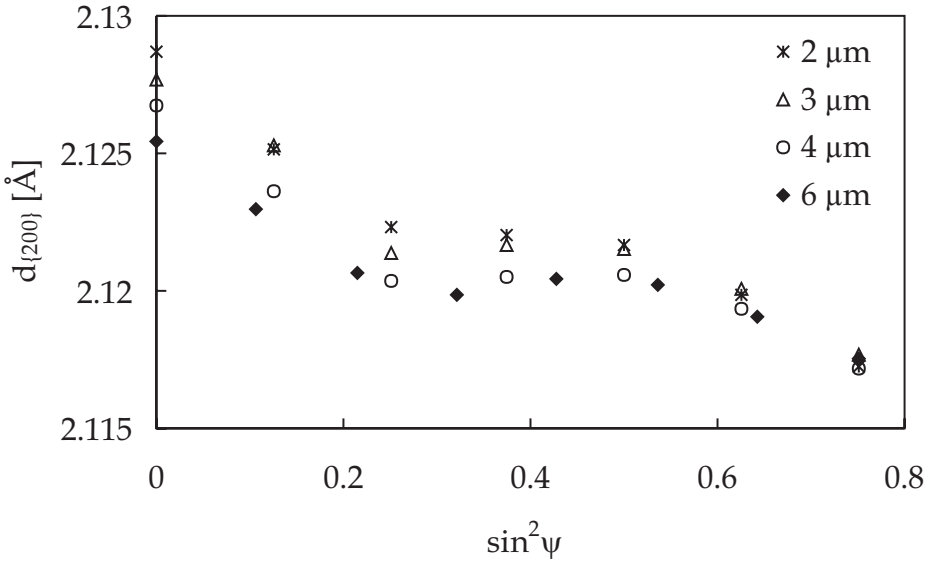

Figure 4.4 Lattice spacings of the {200} planes measured in the rolling direction for the specimens.

and it is not possible to determine the macro residual stresses from the graphs. However, in the transverse direction the relation is linear and is it possible to determine the slopes of the d-$\sin^2\psi$ graphs. Using the Reuss approximation and the elastic compliances from section 3.2, S_{11} =1.8·10^{-12} [m^{2}N^{-1}], S_{12} = -3.2·10^{-13} [m^{2}N^{-1}] and S_{44} = 8·10^{-12} [m^{2}N^{-1}], it is feasible to calculate the stresses. In section 3.2 it was also shown that the relation between the stress in the transverse and rolling direction is $\sigma_{TD} \approx 1.4 \cdot \sigma_{RD}$. Therefore, using the stresses in the transverse direction and this relation makes it possible to determine the stresses in the rolling direction, tabulated in Table 4.2. The stress decreases as the layer thickness increases, meaning that there is a stress gradient present in the layer.

Table 4.2 Experimental and fitted stresses in the rolling direction. $E_{\{200\}}$=565 GPa, $\nu_{\{200\}}$=0.178 and A1=-2.2 [GPa], A2=-3.3 [GPa] and A3=-4*10^5 [µm^{-1}].

Film thickness [µm]	Experimental stress [GPa]	Fitted stress [GPa]
2	-3.9	-3.9
3	-3.3	-3.4
4	-2.9	-3.0
6	-2.5	-2.5

Discussion

The texture and strain measurements on the {200} planes have shown that there is a texture and a stress gradient present in the coating. The {200} planes show a distinct deviation from the linear d-$\sin^2\psi$ relation and there is a relation between the texture and this oscillatory behaviour. The curvature is present for all four specimens and seems to be related to the magnitude of the stresses. In literature there are three main explanations for an oscillatory d-$\sin^2\psi$ behaviour schematically shown in Figure 4.5 [1,2,3].

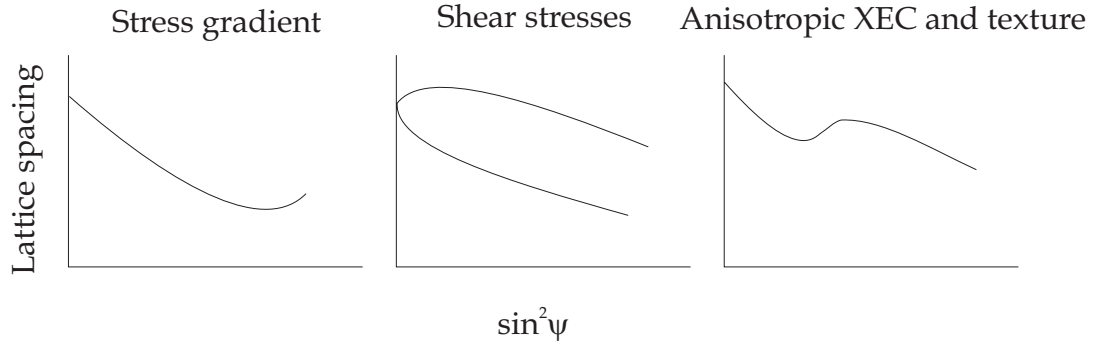

Figure 4.5 Different causes of non-linear d-$\sin^2\psi$ behaviour

1. The influence of the stress gradient is due to the effect that the measured strain is an average value over the penetration depth of the X-rays. Increasing the ψ means that the penetration depth will decrease. During the strain measurements the ψ angle is varied and this will result in a gradually convex or concave curve.
2. The presence of shear stresses can easily be determined. The shear stresses σ_{13} and σ_{23} have a $\sin 2\psi$ influence on the measured d spacing. So a difference between $\psi<0$ and $\psi>0$ means there are shear stresses present.
3. When there is a large difference in X-ray elastic constants, XEC, then the orientation of a specific crystal will determine how the d spacing changes as a function of an applied force [2,3]. When there is also a strong texture present in the material an oscillatory d-$\sin^2\psi$ relation may occur, section 2.3. It can be shown that when the d-spacings of {h00} and {hhh} planes of cubic materials are measured this effect does not occur. The reason is that for these two reflections the s_{33ij}^{lab} term in Equation (2.30) is zero for ij=12, 13 and 23.

The first and the second explanation can be rejected immediately. The curvature that is generated by these causes is reflection independent. They are visible and identical in all the planes. With reference to Figure 4.5, the observed non-linearity has a large resemblance with the shape of the third curve. Besides this there is a strong texture present in the coating and the XEC are very anisotropic. There is, however, one problem: the plane is a {h00} plane and the theory predicts that there is no influence due to the anisotropy visible on this reflection [2]. Therefore, we have to propose another explanation for the non-linear d-$\sin^2\psi$ behaviour. In rolled materials the deformation texture may generate plastic deformation, which may result in an oscillatory behaviour. However, this is only observed for rolled metals [4,5] and it is not the explanation for the oscillatory behaviour observed here.

4.1.2 Stresses in sputtered coatings

The stresses in the deposited layers can originate from the thermal stress and the atomic peening stress [6,7]. The thermal stress in these magnetron sputtered coatings is approximately 400 MPa and is not the main contributor to the total stress in the coating (See previous section).

The peening process, due to the kinetic energy of the incoming atoms and ions, generates a hydrostatic stress in the coating, which induces an expansion of the coating [8]. To make it possible to fit the layer onto the infinitely stiff substrate it is necessary to compress the coating. This will generate a compressive biaxial stress-state in the coating that is related to this hydrostatic stress. It was shown that under certain assumptions the fixation stress in the coating is related to this hydrostatic stress according to:

$$\sigma^{fix} = -\frac{3}{2}\sigma^{hydro} \tag{4.1}$$

There are now three stresses in the coating:

- The hydrostatic stress, σ^{hydro}, which generates the volume expansion. The hydrostatic stress results in a stress state given by $\sigma_{11}=\sigma_{22}=\sigma_{33}$ [9].
- The fixation stress generated by the volume expansion, which is restricted by the substrate. This results in a biaxial stress state.
- The thermal stress, which is also biaxial.

The measured lattice spacing is now derived from Equation (2.24) with the stress components defined above.

$$d_\psi - d_0 = d_0\left[\frac{1+\nu}{E}\left(\sigma^{fix}+\sigma^{ther}\right)\cdot\sin^2\psi - \frac{2\nu}{E}\left(\sigma^{fix}+\sigma^{ther}\right)+\frac{1-2\nu}{E}\sigma^{hydro}\right] \tag{4.2}$$

The question to be addressed is:" How can this lead to a non-linear relation between the d_ψ and the $\sin^2\psi$?"

It was possible to explain the biaxial texture with the difference in sputter yield between aligned and misaligned grains. It is very likely that the process mentioned also has an influence on the atomic peening. For the misaligned grains, much of the energy of the incoming particles is used for resputtering of these grains. Therefore, the amount of particles that will penetrate deep enough is smaller and consequently the atomic peening will be lower than for the aligned grains.

The influence of this process on the *d*-spacing is schematically shown in Figure 4.6. When atoms or ions enter a free-standing grain, this grain will expand and

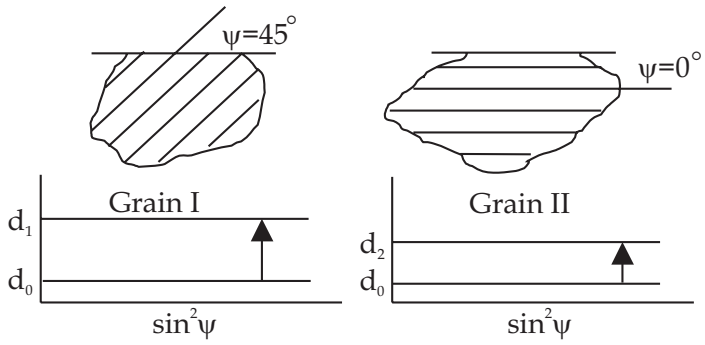

a) A high peening ratio b) A low peening ratio

Figure 4.6 Influence of the grain orientation on the atomic peening and on the lattice spacing.

a compressive stress develops in the grain. The traction at a free surface must be zero, and to fulfil this requirement a tensile force has to be applied [8]. This is the already mentioned hydrostatic stress and is the same in all directions. Due to the hydrostatic stress the lattice spacing of the grain will change and the amount of the change in d_0 is a function of the amount of peening.

Therefore, due to the difference in atomic peening the d_0 is a function of the grain orientation. If the expanded layer is compressed to match onto the substrate all the grains will feel the same compressive force and the measured macro strain will be the same. The consequence of this is that in Equation (4.2) the σ^{hydro} term becomes dependent on the angles φ and ψ, but nothing will change for the σ^{fix}, which is given by the average hydrostatic stress. Equation (4.2) becomes:

$$\frac{d_\psi - d_0}{d_0} = \frac{1+\nu}{E}\left(\sigma^{fix} + \sigma^{ther}\right)\cdot\sin^2\psi - \frac{2\nu}{E}\left(\sigma^{fix} + \sigma^{ther}\right) + \frac{1-2\nu}{E}\sigma^{hydro}(\varphi,\psi) \qquad (4.3)$$

where the $\sigma^{\text{hydro}}(\varphi,\psi)$=P$(\varphi,\psi)\cdot\sigma^{\text{hydro}}$(average), and P is the peening ratio. When the d_ψ is now measured as a function of the $\sin^2\psi$, this will not necessarily yield a straight line.

4.1.3 Calculations

The goal is to calculate the peening ratio and to investigate if there is a relation between the atomic peening and the grain orientation. To simplify this calculation the φ dependence of the peening ratio is neglected and the calculations are performed in the rolling direction. Firstly, it is necessary to find the stress gradient in the coating. With this stress gradient and Equation (4.2) it is then possible to calculate the lattice spacing as a function of the position in the layer. This value must be the same as the measured lattice spacing which is for a ψ goniometer given by:

$$\langle d\rangle_\psi = \frac{\int_0^D d_\psi(z)\cdot e^{-\frac{2z\mu}{\sin\theta\cdot\cos\psi}}\,dz}{\int_0^D e^{-\frac{2z\mu}{\sin\theta\cdot\cos\psi}}\,dz} \qquad (4.4)$$

where μ is the absorption coefficient of TiN and D is the thickness of the coating. From these calculated d-spacings it is then possible to determine the residual stresses, which must correspond to the empirical values of Table 4.2. The shape of the stress is taken as a simple exponential function given by σ^{fit}=A1+A2 $e^{A3\cdot z}$ with z=0 at the interface. With A1= -2.2 [GPa], A2=-3.3 [GPa]

and A3=-4 10^5 [μm^{-1}] the stresses calculated fit the measured stresses of Table 4.2.

Before it is possible to calculate the peening ratios one should realise that Equation (4.4) is correct for a material without a texture gradient. However, the results from Table 4.1 show that there is a texture gradient present and this will change Equation (4.4) into:

$$\langle d \rangle_\psi = \frac{\int_0^D d_\psi(z) \cdot a(z,\varphi,\psi) \cdot e^{-\frac{2z\mu}{\sin\theta\cdot\cos\psi}} dz}{\int_0^D a(z,\varphi,\psi) \cdot e^{-\frac{2z\mu}{\sin\theta\cdot\cos\psi}} dz} \qquad (4.5)$$

Here the function $a(z,\varphi,\psi)$ takes the dependency of the texture with respect to the angles φ and ψ and the depth, z, into consideration. The texture gradient acts as an internal weight for the d-spacing at a specific z. Therefore, it is necessary to find a function to represent the texture gradient. The main points are that the intensity at ψ=0 decreases and the maximum intensity increases with layer thickness, Table 4.1. The texture is composed of two parts: a background which is independent of ψ and which decreases exponentially and a Gaussian peak, which increases linearly with the layer thickness. The weight function is given in Table 4.3 and also the calculated values, which show the same behaviour as the measured ones.

Table 4.3 Calculated intensity with the function:

$$I(z,\psi) = 38 + 0.42 \cdot e^{\frac{(6-z)^3}{28\cdot 10^6}} + (2+z)\cdot 10^{-6} * e^{-0.5\left(\frac{\psi-0.56}{0.1323}\right)^2}$$

	Intensity [a.u.]	
Film thickness [μm]	Maximum	ψ=0
2	1006	177
3	1360	145
4	1719	123
6	2440	100

In Figure 4.7 the measured data-points for the 45 minutes specimen are plotted as a function of the $\sin^2\psi$. The lines are the d values calculated using Equation (4.3) and (4.5) where the solid line is for $\sigma^{hydro}(\varphi,\psi)=\sigma^{hydro}$(average), the dashed-dotted line is for $\sigma^{hydro}(\varphi,\psi)=0.7\cdot\sigma^{hydro}$(average) and the dashed line is for $\sigma^{hydro}(\varphi,\psi)=1.4\cdot\sigma^{hydro}$(average). The calculated lines are not straight which is a consequence of the texture and stress gradient.

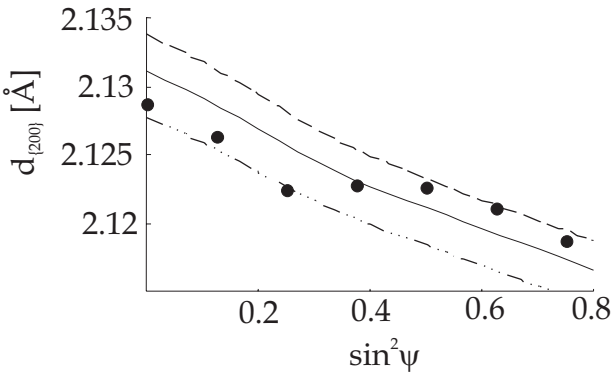

Figure 4.7 Influence of the atomic peening on the lattice spacing. The solid line is for a peening factor of 1, the dotted-dashed lines is for a peening factor of 0.7 and the dashed line is for a peening factor of 1.4.

The results show that a relation between the peening and the grain orientation may explain the non-linear behaviour. The direction in which a preferred growth is found requires a higher peening than that for the other directions.

The peening ratios for the measured data points are determined, Table 4.4, and show the expected behaviour, lower in the beginning and increasing with increasing intensity. Furthermore, there is no difference in peening ratio between the different specimens and this is something that would be expected.

Table 4.4 Fitted atomic peening ratios for the four specimens. Values are for all the specimens approximately the same

	Value peening factor			
$\sin^2\psi$	2 µm	3 µm	4 µm	6 µm
0	0.7	0.6	0.7	0.9
0.125	0.7	0.6	0.6	0.7
0.25	0.7	0.5	0.5	0.6
0.375	1.0	1.0	0.9	1.0
0.5	1.4	1.3	1.5	1.4
0.625	1.4	1.4	1.5	1.4
0.75	1.4	1.3	1.3	1.2

Conclusions

The X-ray diffraction results show that the coatings have a crystallographic texture and that due to the atomic peening process a stress is present in the

layers. The texture and the stress change as a function of the layer thickness and assuming the picture at a lower thickness is preserved for longer deposition times validates the conclusion that in a layer both a texture and a stress gradient exists. The strain measurements on the {200} planes show an oscillatory d-$\sin^2\psi$ behaviour, which cannot be explained by the well-known causes for an oscillating d-$\sin^2\psi$ behaviour, namely the presence of shear stresses or a stress gradient. The non-linearity appears to have a relation with the texture evolution, indicating a connection between both phenomena. Assuming that the texture is determined by the ion-bombardment, the possibility exists that the atomic peening process is also influenced by this ion-bombardment. This will result in a peening ratio, which depends on the grain orientation. As a consequence of this the unstrained lattice spacing will also depend on the grain orientation. Therefore, plotting the d-spacing versus the $\sin^2\psi$ can result in an oscillatory graph.

4.2 X-ray diffraction on a free-standing TiN coating

Introduction

The results of diffraction experiments carried out on a thin film on a substrate of a different material may be significantly influenced by the substrate. Substrate reflections may interfere with reflections of the coating and, depending on the deposition process, residual stresses can develop in the coating. In this section diffraction experiments are performed on a TiN layer deposited on a tool substrate with an interface roughness of 0.1 μm R_a. After the measurements the tool steel substrate underneath the TiN coating is removed and the diffraction measurements are repeated. Comparing the results makes it possible to draw some conclusions about the influence of the substrate on diffraction experiments. The structure of this commercially manufactured coating is comparable to that of the third batch, a columnar {111} fibre texture, with high residual stresses. (See also chapter 5 and 6.)

4.2.1 Experimental procedure

The tool steel substrate is removed in two steps: firstly the bulk of the substrate is removed by grinding and polishing and the second and final step is to chemically etch away the remaining substrate. The TiN layer is then glued onto a glass plate using an amorphous adhesive. Care is taken to assure that the orientation of the TiN layer on the glass plate is the same as it was on the substrate. This is checked by looking at the texture, which should be, when the orientation is still the same, a {111} fibre texture.

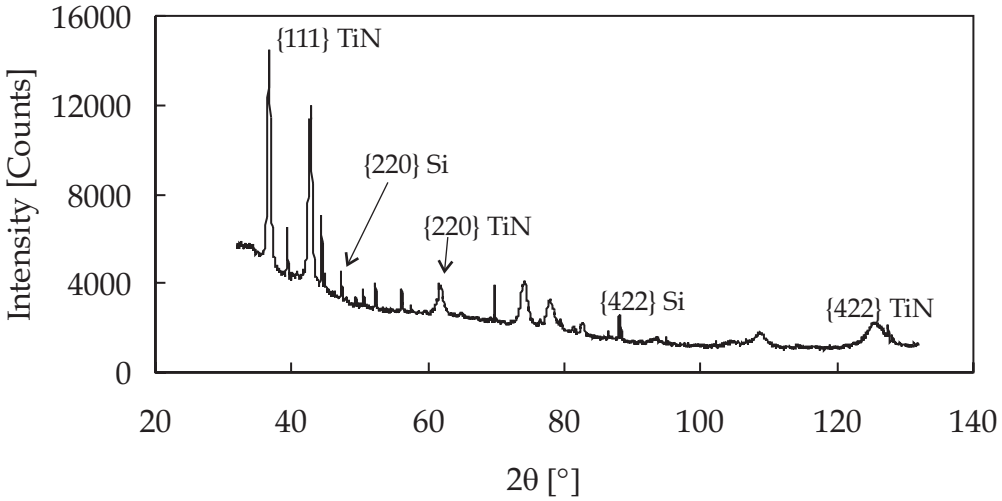

Figure 4.8 Diffraction pattern of the free-standing TiN film. The amorphous background is of the adhesive and the very small peaks are of the added silicon powder.

The diffraction pattern of the free-standing coating is presented in Figure 4.8. The large amorphous background is due to the adhesive and the glass plate. Diffraction peaks of the TiN and of Silicon powder are visible and the results show that nearly all the substrate is removed, that is no iron peaks are present.

In section 2.2.4 it was mentioned that displacement of the specimen from the diffractometer axis might have a large influence on diffraction experiments. Especially, for a free-standing layer this may cause a significant error. This problem can be minimised by performing the measurements for small ψ's and higher order planes. This is the reason why only the results for ψ<55° are considered and to determine the macro residual stresses the {422} planes are used.

4.2.2 Diffraction experiments

Macro residual stress

Firstly, the residual stresses in both specimens are determined. The measured lattice spacings of the {422} planes are plotted in Figure 4.9. The slope of the as deposited coating is much steeper than that of the free-standing layer. To be able to calculate the stress from this slope the XEC are needed. However, their exact values are for these commercial layers not known and to get around this problem of the XEC, the slope of the lines is divided by their intercept with the

ordinate. This gives a value, which is the residual stress divided by $\frac{1}{2}S_2$. This value is for the as deposited coating $-9.78 \cdot 10^{-3}$ and is a factor of 8 smaller for the free-standing layer, $-1.23 \cdot 10^{-3}$. So nearly all the residual stresses have disappeared. If the substrate is removed, the coating is free to expand and the long-range residual stresses will disappear. However, this does not mean that the cause of the original stresses, i.e. due to the peened atoms, is removed as well.

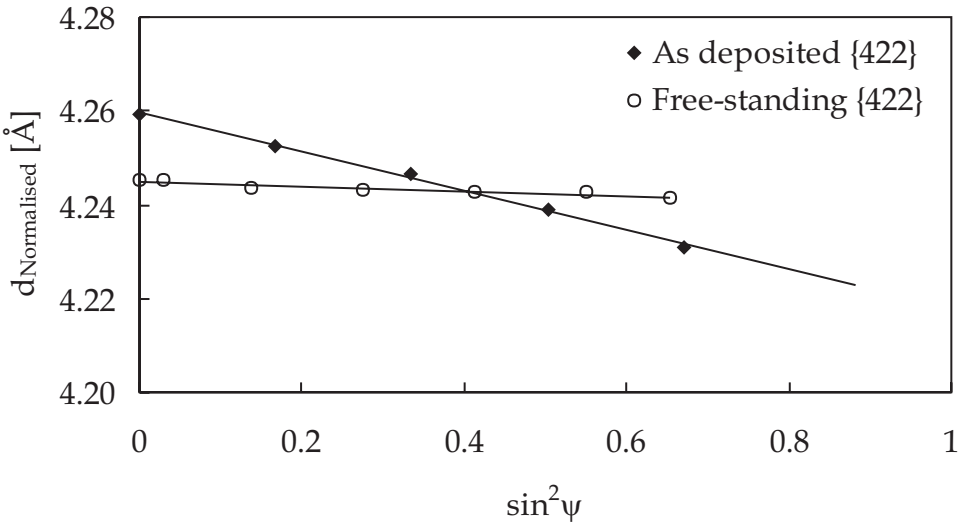

Figure 4.9 Lattice spacing of the {422} planes in the as deposited and in the free-standing coating. Due to the removal of the substrate most of the residual stresses have disappeared.

In Figure 4.10 the lattice spacings of the {200} planes for the as deposited and the free-standing layer are plotted versus the $\sin^2\psi$. The graph of the as deposited layer shows a small deviation from a linear relation and this is only present in the beginning of the graph. This curvature is also visible in the {200} planes of the specimens from the third batch. This was the reason why for the {200} planes of Figure 3.12 no point is plotted at ψ=0. The graph of the free-standing layer is strongly curved over the entire $\sin^2\psi$ range. This curvature is not a consequence of a displacement from the diffractometer axis only. This can be concluded from the fact that the error due to this displacement should decrease with increasing 2θ (See Table 2.3). Comparing the results from the {400} planes, 2θ=93.218°, and the {220} planes, 2θ=61.856°, shows that the curvature of the {400} planes is much larger than the curvature in the {220} planes.

If the data from the free-standing layer are taken as the starting point the question is whether or not it is possible to recalculate the lattice spacings of the {200} planes of the as deposited layer? If this is the case then the curvature is an intrinsic property of the coating. The lattice spacing as a function of the ψ angle and the residual stress σ, assuming a biaxial symmetrical stress-state, is given by:

$$d_\psi = d_\psi^{Free\,standing}\left[\tfrac{1}{2}S_2\cdot\sigma\cdot\sin^2\psi + 2S_1\cdot\sigma\right] + d_\psi^{Free\,standing} \tag{4.6}$$

The $d_\psi^{\text{Free-standing}}$ is the lattice spacing of the free-standing layer as a function of the angle ψ. To find this value over the entire interval, a polynomial of the fourth order is fitted through the measured points. Fitting the strain and not the stress can partly circumvent the problem of the XECs. The only problem is then the term $-2S_1\cdot\sigma$, but this is a term, which is independent of ψ and only influences the intercept with the ordinate. This value is also fitted. The crosses in Figure 4.10 are the fitted data which have a correlation coefficient of 0.97 and the fitted term, $\frac{1}{2}S_2\cdot\sigma$, is $-8.25\cdot10^{-3}$. This value is just slightly smaller than the difference in the values obtained from the {422} planes, $-8.55\cdot10^{-3}$. This difference can be a consequence of two effects. Firstly, a difference in XEC and

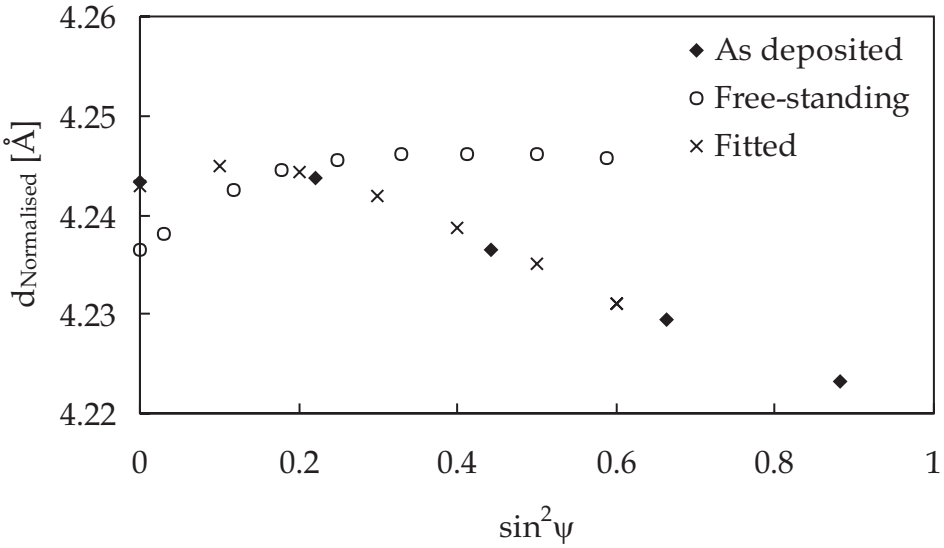

Figure 4.10 Normalised lattice spacing of the {200} planes in the as deposited and in the free-standing coating. A polynomial of the fourth order is fitted, not shown, through the data points of the free-standing coating. With this function and assuming a biaxial state of stress it is possible to fit the stress so that the points calculated from this function agree with the measured data of the as deposited coating.

secondly, using a different plane means measuring at a different 2θ angle, which changes the information depth.

There are two main conclusions that can be drawn from the performed experiments:

- The residual stresses in the free-standing layer are considerably lower than in the as deposited layer, approximately 1/8 of the initial residual stress is still present [10].
- The removed stresses where perfectly biaxial and there appears to be a relation between the unstrained lattice spacing of the {200} planes and the direction in which they are measured.

Deformation strain and grain size

The Williamson-Hall plots of the specimens, Figure 4.11, show that there is no large difference between the peak width of both specimens [10,11]. The difference between the deformation strain, $7.0 \cdot 10^{-3}$ for the as deposited and $6.7 \cdot 10^{-3}$ for the free-standing layer is within the experimental error. The intercepts with the ordinate, $-5.5 \cdot 10^{6}$ and $-1.5 \cdot 10^{6}$ for the as deposited and for the free-standing layer, respectively, are again negative and have as such no physical meaning. The macro stress in the free-standing specimen is almost

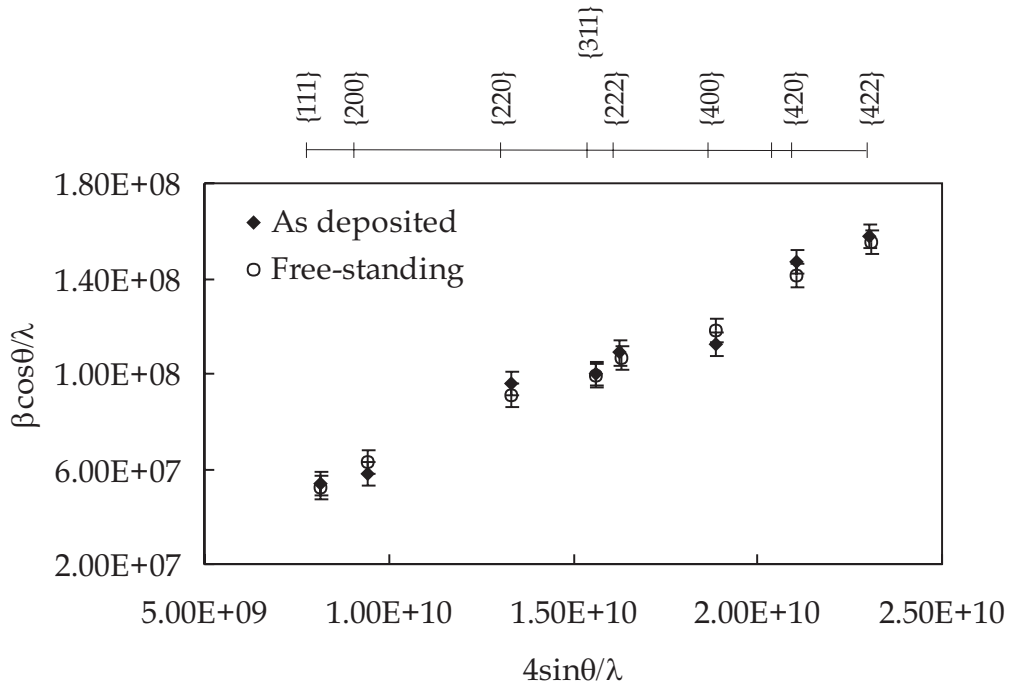

Figure 4.11 Williamson-Hall plots for the as deposited and the free-standing coatings. There is no difference visible.

completely removed and the conclusion that the macro stress gradient, that might still be present in the layer, is negligibly small appears to be justified. The consequence of this is that the width of the diffraction peaks is not due to the presence of a gradient in the macro residual stress as was suggested in section 3 of chapter 3.

Nelson-Riley plot

From the measured peak positions the lattice spacings are calculated and these data are plotted versus $\cot\theta \cdot \cos\theta$. The data of the silicon powder are used to determine the systematic error in the experiments. The data from the free-standing TiN are corrected for this systematic error. The results of the as deposited TiN coating and the free-standing layer are plotted in Figure 4.12. The Nelson-Riley intercepts are determined for both the specimens and this is done for three different cases: using all the reflections, only the {111} and {222} reflections and using only the {200} and {400} reflections (See Table 4.5).

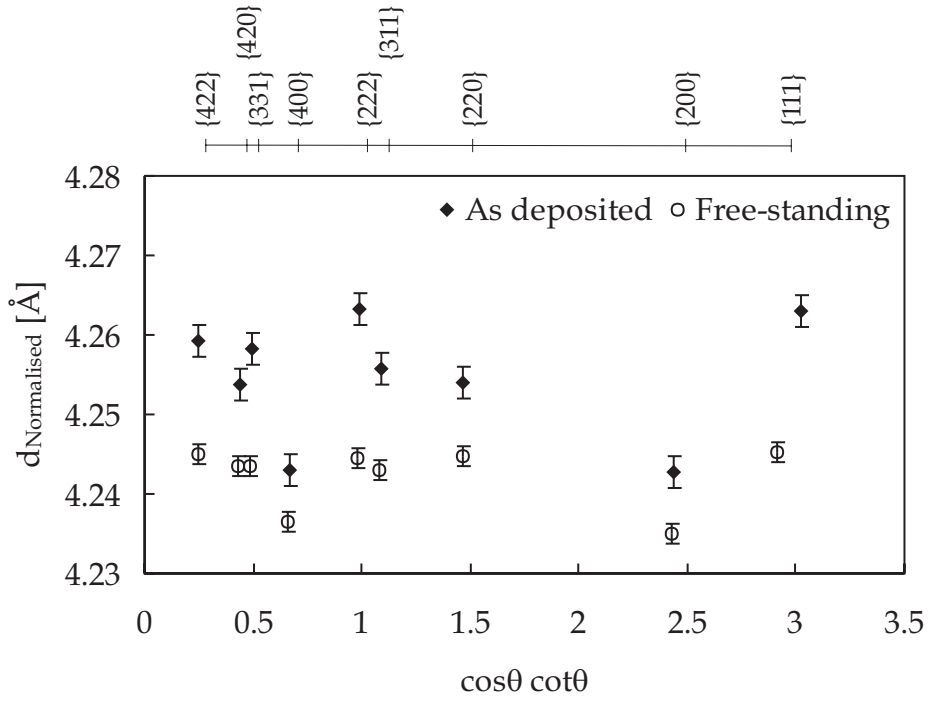

Figure 4.12 Nelson-Riley plots for the as deposited and the free-standing coatings. Due to the lower macro residual stress, the values for the free-standing coating are smaller. There appears to be less dispersion between the reflections of the free-standing layer.

There are two points worth mentioning when the results of the as deposited coating are examined. The lattice spacing found using all the points is much larger than the theoretical value for stoichiometric TiN, 4.2392 Å [12], and there is a distinct difference between the {hhh} and the {h00} reflections. The first point can be explained by looking at the residual stresses that are present in the coating. These stresses are compressive and the outcome is that the spacing between planes parallel to the interface will be larger. The difference between the {hhh} and {h00} reflections can also be a consequence of these residual stresses. As mentioned before, the XEC for these two planes are different and assuming that the stresses are the same in all the crystals may explain this result. The results of the free-standing coating show an intercept, that is much smaller and there is still a difference visible between the intercepts of the {hhh} and the {h00} reflections. The lower intercept is a direct consequence of the removed substrate. The coating is no longer contracted by the substrate and the coating will expand in the plane of the coating and shrink in the direction perpendicular to the layer. The residual stresses determined in the previous section are still not completely zero. So the value is still not the true unstrained lattice spacing.

Table 4.5. Lattice spacing determined with a Nelson-Riley plot.

	lattice spacing [Å]		
	All reflections	{111} and {222}	{200} and {400}
As deposited TiN	4.2551	4.2634	4.2433
Free-standing TiN	4.2431	4.2442	4.2370
Extrapolated to σ=0	4.2414	4.2415	4.2361

The difference in intercept between the {hhh} and the {h00} reflections of the free-standing layer, 0.0072 Å, is smaller than the difference for the as deposited coating, 0.02 Å. This decrease is probably due to the decrease in macro stress in relation with an anisotropy in the XEC. From these data it is not possible to calculate the anisotropy factor.

Despite the fact that part of the difference between the {hhh} and the {h00} can be explained, there is still a difference, which has a different cause. Extrapolation of the lattice spacing for the three cases to a value of zero macro residual stress results in the data given in the last row of Table 4.6. The lattice spacings obtained using all the reflections and only the {hhh} reflections are the same and this is expected. However, there remains a difference of ≈0.0054 Å between the {hhh} and the {h00} reflections. This is solely a result of a deviation in the {h00} reflections as was also apparent from the macro stress measurements on these coatings.

Conclusions

Diffraction experiments are carried out on an as deposited and on a free-standing TiN coating. The results show that by removing the substrate, the coating can relax and the macro residual stresses disappear. Removing the substrate has no noticeable influence on the deformation strain in the coating. Using a Nelson-Riley plot and extrapolating the data to a value of zero macro stress results in an unstrained lattice spacing of 4.2414±0.0002 Å. The lattice spacings of the {200} planes show a behaviour that deviates from all the other planes and this is visible in the Nelson-Riley plot as well as in the macro residual stress measurements. The XECs of the commercially produced TiN coating are anisotropic but from the present results it is difficult to determine an exact value for the anisotropy factor.

4.3 Influence of annealing on macro residual stresses and deformation strain

As pointed out, there are many different causes of peak broadening and besides this there are also effects that may distort the result obtained. To be able to come to reliable conclusions it is necessary to study the different causes in more detail. In the first part of this section, the different causes for peak broadening are studied and with the results from earlier section some conclusions are drawn. In the second part annealing experiments are performed and the influence of this on the peak position and profile is investigated.

4.3.1 Theoretical survey

The phenomena that generate peak broadening can roughly be divided into two groups, namely effects that generate a direct broadening: finite grain size, lattice defects and concentration gradient, and effects that distort or indirectly influence the broadening: macro stress gradient or anisotropic XECs. The influence of the XECs is already treated in section 3.3.

The measured peak position is always an integrated value over the penetration depth of the X-rays. When the peak position changes as a function of depth, i.e. there is a strain gradient present, this will automatically result in a peak broadening. The effect this will have on the peak broadening can be determined using the strain gradient described in section 3.2.1. The effect is not very large and the broadening is for this particular case asymmetrical [13]. The influence the strain gradient has on the peak profile can also be estimated from the results of the previous section. The peak profiles of the as coated and the free-standing layer where comparable although the macro stress in the free-standing coating

was almost zero. So this means no gradient present anymore. Therefore, this effect does not play a significant role in the peak broadening.

For the true broadening phenomena there are four questions that must be addressed when studying the broadening effects:

- How does the phenomenon manifest itself?
- How strong is the effect?
- What is the relation between the broadening and the different reflections, i.e. the relation between the broadening and the θ angle?
- Is there a relation between the phenomenon and the deposition parameters?

Grain size

Starting with the grain size [14,15], this results in a broadening for all the reflections but the peak position stays the same. This effect is especially visible when the grains are small, <<1000nm. The relation between the broadening and the θ angle is covered by Equation (2.16). It seems plausible that the deposition parameters have an influence on the grain size. For example, decreasing the bias voltage will result in a coarsening of the grain size. However, as was already pointed out, it is not possible to obtain a reliable value for the grain size with X-ray diffraction.

Concentration variation

The lattice spacing of TiN_x is related to the amount of nitrogen and it is possible that this concentration is not constant throughout the coating. This will result in a peak broadening as well. To determine the influence of the concentration gradient Bragg's law is written in an adapted form:

$$\theta = \arcsin\left[\frac{\lambda \cdot \sqrt{h^2+k^2+l^2}}{2 \cdot d_0}\right] \tag{4.7}$$

Assuming that the error in the lattice spacing, Δd, is small then Equation (4.7) can be differentiated with respect to d.

$$\frac{\Delta\theta}{\Delta d} = \frac{\lambda\sqrt{h^2+k^2+l^2}}{2 \cdot d_0 \sqrt{1-\dfrac{\lambda^2\left(h^2+k^2+l^2\right)}{4d_0^2}}} \longrightarrow \Delta\theta = \frac{\Delta d}{d_0}\tan\theta \tag{4.8}$$

A concentration variation, Equation (4.8), has exactly the same influence on the peak broadening as the deformation strain, Equation (2.20). Therefore, the slope

of the line obtained with the Williamson-Hall plot does not only contain information about the deformation strain but also about a possible concentration variation. The influence of a concentration variation can readily be estimated. A concentration variation with a Cauchy profile generates a Williamson-Hall plot with the slope given by $\Delta d/4 \cdot d$. Assuming that there is a variation in the nitrogen concentration of 20 atom%, i.e. a Cauchy profile with a FWHM of 0.005Å [12], results in a slope of $\approx 3 \cdot 10^{-4}$. This value is a factor of ten smaller than the measured slope. Therefore, the conclusion is that a concentration variation may play a role in the peak broadening but the influence is negligible.

Lattice defects

The lattice defects that are considered here are stacking faults, twin faults, point defects and dislocations. Starting with the stacking and twin fault densities. The twin faults produce an asymmetrical peak broadening, whereas stacking faults produce a peak shift and a symmetrical peak broadening [16,17,18,19]. The technique developed by J.B. Cohen to determine the twin fault probability is to determine the peak position with the centre of gravity method, COG. Due to the asymmetry, the found peak position will differ from the true peak position. This shift is then a measure for the twin fault probability. The influence these twin faults have on the ΔCOG is given by:

$$\begin{aligned} \Delta COG_{111}[^\circ 2\theta] &= +11 \cdot \gamma \cdot \tan\theta_{\{111\}} \\ \Delta COG_{200}[^\circ 2\theta] &= -14.6 \cdot \gamma \cdot \tan\theta_{\{200\}} \end{aligned} \qquad (4.9)$$

(γ is the twin fault probability.) These equations show that the influence is different for different reflections. The stacking fault probability is best determined by measuring the displacement of the peak maxima from those of an annealed specimen. (This shift is not the same for different reflections.) The broadening due to the stacking faults is exactly the same as the broadening due to a finite particle size. (That is the reason why the peak shift is used for determining the stacking fault probability.) It seems reasonable that stacking and twin fault broadening play a role in the sputtered TiN coatings. Therefore, these phenomena can influence the peak width of different reflections but will not have a significant influence on the slope of the Williamson-Hall plot. There is no clear relation between the stacking and twin fault probability and the deposition parameters. Therefore, these effects do not induce the increase in slope of the Williamson-Hall plots of the specimens with a higher macro stress.

From the survey above it seems permissible to assume that point defects and dislocations are to a large extent responsible for deformation strain in the

specimens. It is possible to estimate the dislocation density from the measured deformation strain [20,21]. The deformation energy is given by:

$$E_{strain} = A \cdot E \cdot \xi^2 \tag{4.10}$$

Where A is a factor, which depends on the shape of the strain distribution, E is the Young's modulus and ξ is the deformation strain. The energy of a single dislocation in a crystal is:

$$E_{dislocation} = K \cdot \ln \frac{R}{r_0} \tag{4.11}$$

The pre-logarithmic factor K is the energy term, r_0 the repulsion core radius and R is the crystal radius. The interaction of dislocations will influence the strain energy term by a factor F. Assuming the total strain energy in a crystal is generated by the dislocation, makes it possible to relate the measured deformation strain to the dislocation density ρ.

$$\rho \propto \frac{1}{F} \cdot \frac{\xi^2 \cdot}{\bar{b}^2} \tag{4.12}$$

Calculating the dislocation density is now possible when the dislocation interaction term F is known. This F is influenced by pile-ups and sub-cell formation. The pile up of dislocations against barriers in the slip plane causes a change in the strain energy per dislocation. A decrease in strain energy per dislocation can arise by polygonization, sub-cell formation. The dislocations climb from their bend planes to form slip planes cancelling their long-range stress fields.

Calculating the dislocation density in the specimens with the highest deformation strain, $1 \cdot 10^{-2}$, results in a dislocation density of 10^{16} [m^{-2}]. For highly deformed metals, the dislocation density is on average between 10^{14} to 10^{16} dislocations per square meter. The found value is comparable to that of highly deformed metals and the question that arises:" Is this possible for ceramic TiN films?"

4.3.2 Annealing experiments

Introduction

A material that experiences either a residual stress or a deformation strain is thermodynamically unstable. By heating, it is possible to transform the material

to a state of lower energy. There are three principal processes that may occur during the heat treatment of a material [22]:

- Recovery. This stage is characterised by the reduction of the dislocation density and the rearrangement of the remaining dislocations. The dislocations can be rearranged in well-defined sub grains and this is called polygonization.
- Recrystallization. The nucleation and growth of new strain free grains.
- And finally grain growth. When the material contains only strain free grains the average grain size may further increase during annealing.

The division into the three stages is derived from the behaviour of a cold worked metal in an annealing treatment but the question is whether or not this definition is an appropriate physical picture for the ceramic TiN coatings? Estimation of the dislocation density indicates that the TiN films possess a dislocation density, which is comparable to that of a cold worked metal. The macro residual stresses are also very high. Hence the material must be thermally very unstable and a response to an annealing treatment may exhibit a similar behaviour as that defined above.

To study the nature of the curved d-$\sin^2\psi$ and to investigate the high deformation strain that is present in the TiN films, the different specimens of the third batch are annealed in a vacuum furnace with a pressure of $1 \cdot 10^{-5}$ bar. The annealing time, multiples of 12 hours, and the annealing temperatures, 673, 773 and 873 K, were varied. After the annealing steps, the specimens were again thoroughly investigated using X-ray diffraction. Because the specimens from this batch are not the same, i.e. there was a difference in titanium concentration during the deposition process, the annealing treatment at 873 K for 24 hours is carried out on the 40% and the 70% titanium specimens. The results do not

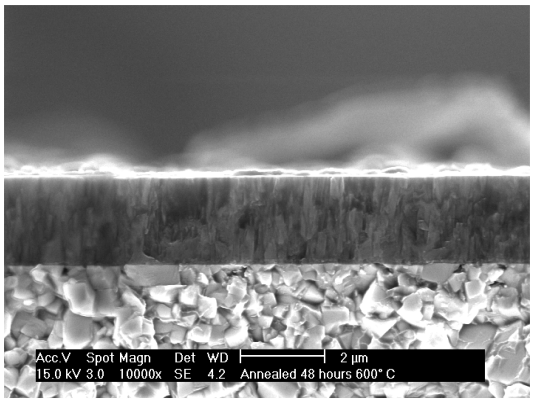

Figure 4.13. SEM micrograph of the specimen annealed at 600° C for 48 hours. There is still a columnar microstructure visible.

differ among each other. From this it may be concluded that the difference in deposition condition does not significantly influence the outcome of the annealing experiments. Therefore the specimens can be considered to be equal.

Annealing process

Firstly it is necessary to determine which of the three process, recovery, recrystallization or grain growth, is dominant in the annealing experiments. The specimen that is annealed for 48 hours at 873 K is examined in an SEM. The micrograph in Figure 4.13 shows that there is still a columnar microstructure present and it appears that no significant recrystalization occurred. This is confirmed by X-ray measurements. When recrystallization takes place the integrated intensity of the diffraction peaks will change because the newly formed grains may have a different orientation. On the other hand during the recovery stage the removal or rearrangement of dislocations will only have an influence on the width and the height of the diffraction peaks but not on their integrated intensities. Figure 4.14 shows that the width of the diffraction peak is decreased and its height increased such that the integrated intensity is still the same. From this it may be concluded that recovery is the dominant process during the annealing experiments.

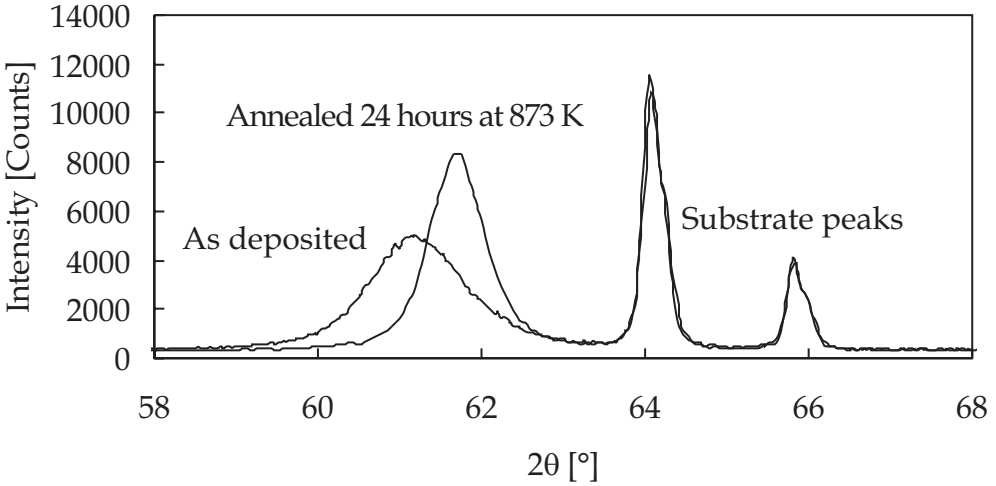

Figure 4.14. Diffraction patterns of the {220} reflection of TiN before and after annealing at 873 K for 24 hours. The peak width has decreased and the peak height has increased so the integrated intensity is still the same.

Macro residual stress

To determine the macro residual stress the peak shift of the {220} planes is measured and using the XEC of section 3.2 enables the calculation of the macro residual stresses. The influence of the annealing experiments on the residual stresses is shown in Figure 4.15. It is clearly visible that the annealing treatment has lowered the residual stress. There is also a relation between the decrease and the annealing temperature, i.e. the stress relaxation is higher for the specimens annealed at a higher temperature. These results are in agreement with results from literature [11,23,24].

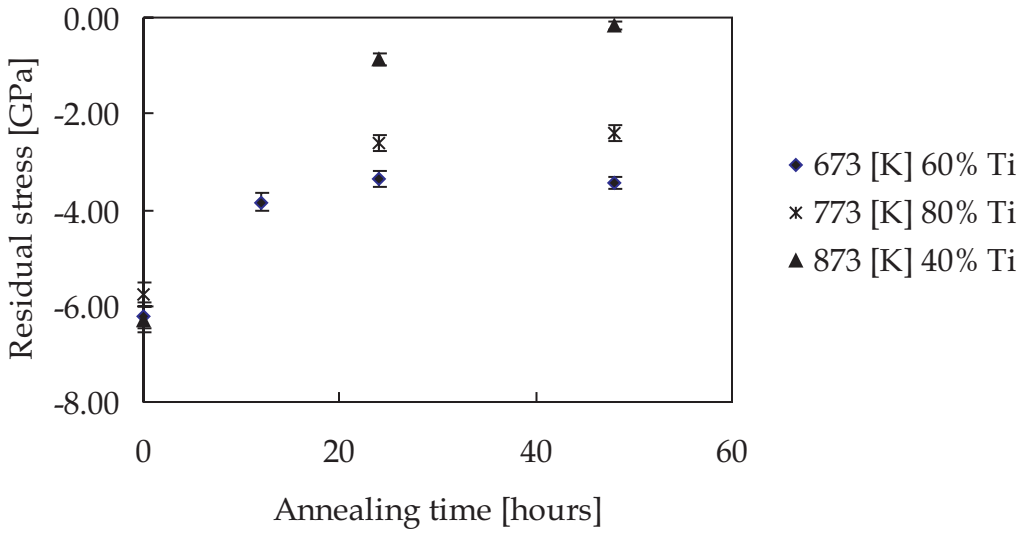

Figure 4.15. The macro residual stresses are plotted as a function of the annealing times and temperatures.

In Figure 4.16 the lattice spacings of the {200} planes of the as deposited and the annealed specimen are plotted versus the $\sin^2\psi$. Using the data from the annealed specimen and applying a biaxial state of stress it is possible to recalculate the graph of the as deposited specimen. So the curved relation that is present is an intrinsic property of the {200} planes and is not a consequence of the high residual stresses and the anisotropic XECs. Removal of the substrate or an annealing treatment produces the same change in state of stress of the coatings.

A question that should be addressed is whether or not this relaxation process is also responsible for the difference in macro residual stress between the coatings with a different deposition time? (The TiN films from the second batch.) The films were deposited at a temperature of 620 K. This is lower than the lowest

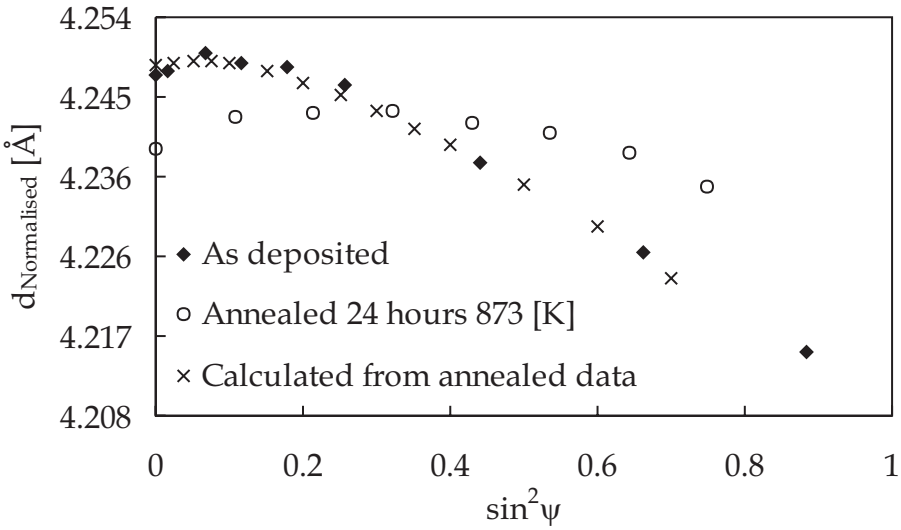

Figure 4.16. The lattice spacing of the {200} planes is measured before and after the annealing treatment. Fitting a fourth order polynomial through the data of the annealed specimen and assuming a biaxial state of stress makes it possible to recalculate the data before the annealing treatment.

annealing temperature, which was 673K. When the data of the annealing experiments of the 60% Ti specimen are used it is possible to calculate the maximum stress relaxation that has occurred after one hour, i.e. -0.5 GPa. This value is smaller than the difference between the specimens with a deposition time of 30 and 90 minutes, -4.5 and –2.6 GPa, respectively. Therefore, a thermal relaxation process is not responsible for the difference in macro residual stress between the specimens from the second batch.

Deformation strain

The influence of annealing on the deformation strain is essentially the same as for the macro residual stress. The deformation strain decreases and the decrease is related to the annealing temperature and time (Figure 4.17). According to Ref [22] is X-ray line broadening affected by recovery processes. The change in this property due to the annealing of a cold worked metal in the recovery stage shows the same behaviour as presented in Figure 4.15 and 4.17. The rate of change is highest in the beginning and at longer times the property approaches the equilibrium value very gradually. Therefore, it seems logical to assume that the high deformation strain that is present in these TiN layers is indeed a consequence of a very high dislocation density. So during the annealing treatment the rearrangement of the dislocation by means of glide and climb will

result in a decreased peak width. It is also clear that the deformation strain is not responsible for the curved d-sin$^2\psi$ behaviour of the {200} planes. The deformation strain is considerably reduced but the non-linearity is still present (Figure 4.16).

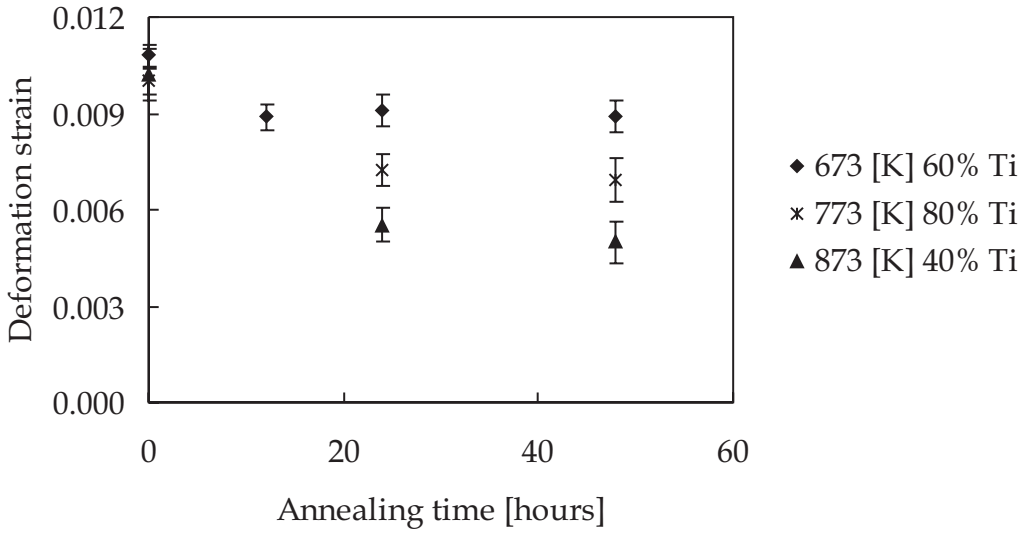

Figure 4.17. The deformation strain plotted as a function of the annealing time and temperature. The same behaviour as for the macro residual stress is present.

Conclusions

Probably dislocations generate the high deformation strain that is present in both the commercial coatings and in the coatings from the third batch. Calculating the dislocation density from the deformation strain results in a value that is comparable to that found for heavily deformed metals. All the specimens with a high deformation strain (the commercial and non-commercial films) also have a curved d-sin$^2\psi$ relation for the {200} planes. To investigate this, some of the specimens are annealed in a vacuum furnace at different temperatures and during different time intervals. The recovery of the TiN films shows the same features as are observed for the annealing of cold worked metals. The deformation strain is decreased and this decrease is highest in the beginning while at longer times the equilibrium value is approached very gradually. Also the macro residual stress is decreased and shows the same dependence on time and temperature as the deformation strain. The curved d-sin$^2\psi$ relation is still present and the relaxation of the macro residual stress is

comparable to that found in section 4.2 (removal of the substrate). More research is needed to fully comprehend the curved d-$\sin^2\psi$ relation.

References

1 I.C. Noyan, J.B. Cohen, Residual Stress, Springer Verlag, New York, 1987.
2 H.J. Dölle,. Appl. Crystall. 12 (1979). 489.
3 P. van Houtte, Mat. Sci. Forum 133-136 (1993) 97.
4 L. Pintschovius, V. Hauk, W.K. Krug, Mat. Sci. Eng. 92 (1987) 1.
5 R.H. Marion, J.B. Cohen, Advances in X-ray analysis 18 (1957) 466.
6 A.J. Perry, J. Vac. Sci. Technol. A 8(4) (1990) 3186.
7 F.M. D'Heurle, J.M.E. Harper, Thin Solid Films 171 (1989) 81.
8 J.D. Kamminga, Th.D. de Keijser, R. Delhez, E.J. Mittemeijer, Thin Solid Films 317 (1998) 169.
9 S. Timoshenko, J.N. Goodier, Theory of elasticity, McGraw-Hill Book Company inc. Tokyo Japan (1934).
10 D.S. Rickerby, J. Vac. Sci. Technol A4(6) (1986) 2809.
11 A.J. Perry, M. Jagner, Thin Solid Films 171 (1989) 197.
12 S. Nagakura, T. Kusunoki, F. Kakimoto, Y. Hirotsu, J. Appl. Cryst.8 (1975) 65-66.
13 J.D. Kamminga, Origin and Measurements of Stresses in Thin Layers, Ph.D. Thesis Delft 1999.
14 B.D. Cullity, Elements of X-ray diffraction, Addison-Wesley, Reading, Massachusetts, 1978.
15 G.K. Williamson, W.H. Hall, Acta Metall. 1 (1953) 22.
16 M.S. Paterson, J. Appl. Phys. 23(8) (1952) 805.
17 B.E. Warren E.P. Warkois, J. Appl. Phys. 24(7) (1953) 951.
18 C.N.J. Wagner, Acta. Metall. 5 (1957) 477.
19 J.B. Cohen C.N.J.Wagner, J. Appl. Phys. 33(6) (1962) 2073.
20 G.K. Williamson R.E. Smallman, Phil. Mag.1, (1956) 34.
21 M. Wilkens, J, Appl. Cryst. 12 (1979) 119.
22 Metals Handbook 9th edition Vol 9. Metallography and microstructures. American Society for metals, Ohio, United States of America.
23] V. Valvoda, R. Cerny, Thin Solid Films 170 (1989) 201.
24 T. Matsue, T. Hanabusa, Y. Ikeuchi, Thin Solid Films 281-282 (1996) 344.